Supplemental file for

Drivers of the $\delta^{18}O$ Changes in Indian Summer Monsoon Precipitation between the Last Glacial Maximum and Pre-industrial Period

Thejna Tharammal [1*], Govindasamy Bala[2], Jesse Nusbaumer[3]

[1] Interdisciplinary Centre for Water Research, Indian Institute of Science, Bengaluru 560012, India

[2] Centre for Atmospheric and Oceanic Sciences, Indian Institute of Science, Bengaluru 560012, India

[3] National Center for Atmospheric Research, Boulder, USA

Corresponding author: thejnat@iisc.ac.in

Contents:

Figures S1-S11,
Tables S1-S2.

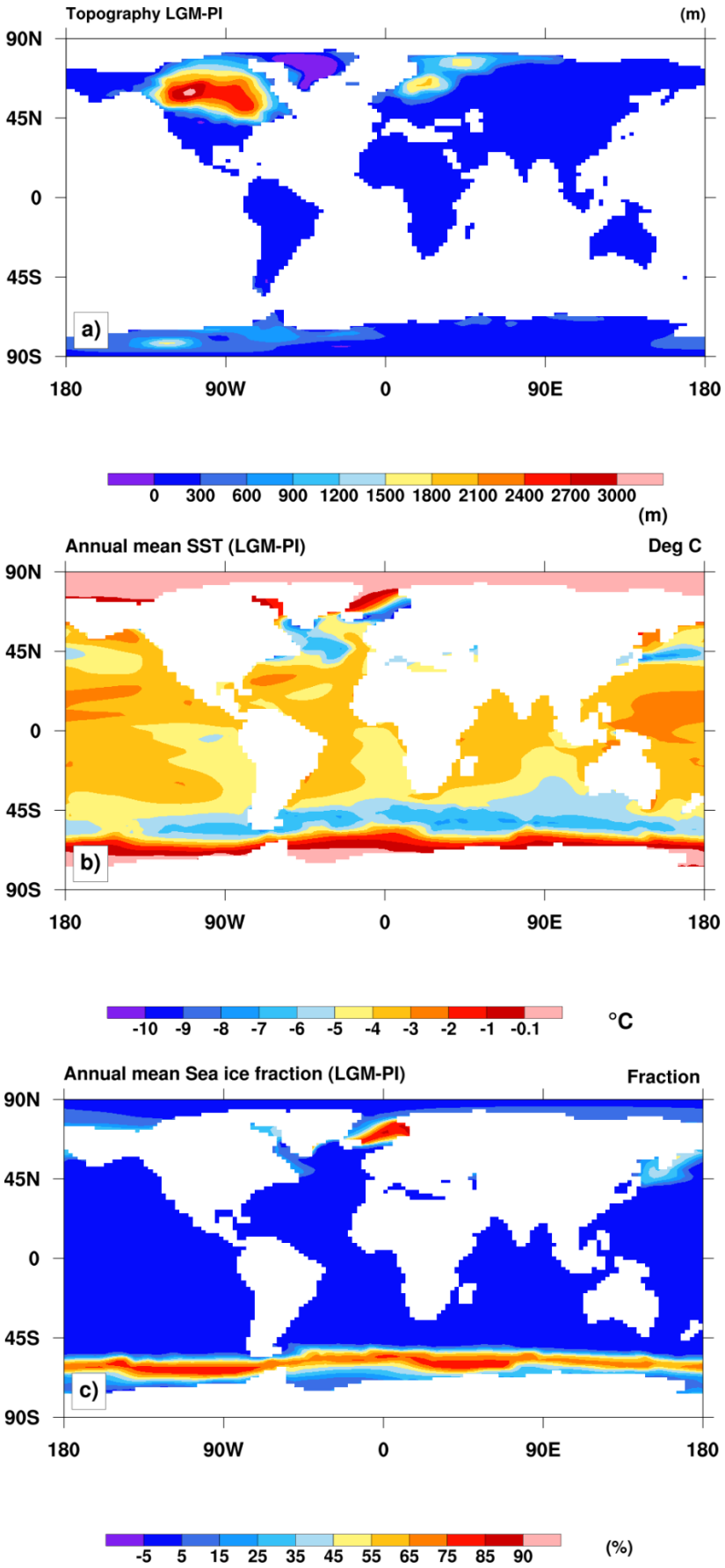

Figure S1. Differences in the boundary conditions between the Last Glacial Maximum (LGM) and Pre-Industrial (PI) simulations. Panel (a) shows the difference

in topography and ice sheet elevation (LGM - PI) in meters (m), highlighting the elevation of the Laurentide and Fennoscandian ice sheets. Panel (b) shows the cooling of annual mean sea surface temperature (SST) (LGM - PI) in degrees Celsius (°C). Panel (c) shows the differences in the sea-ice fraction in percentage.

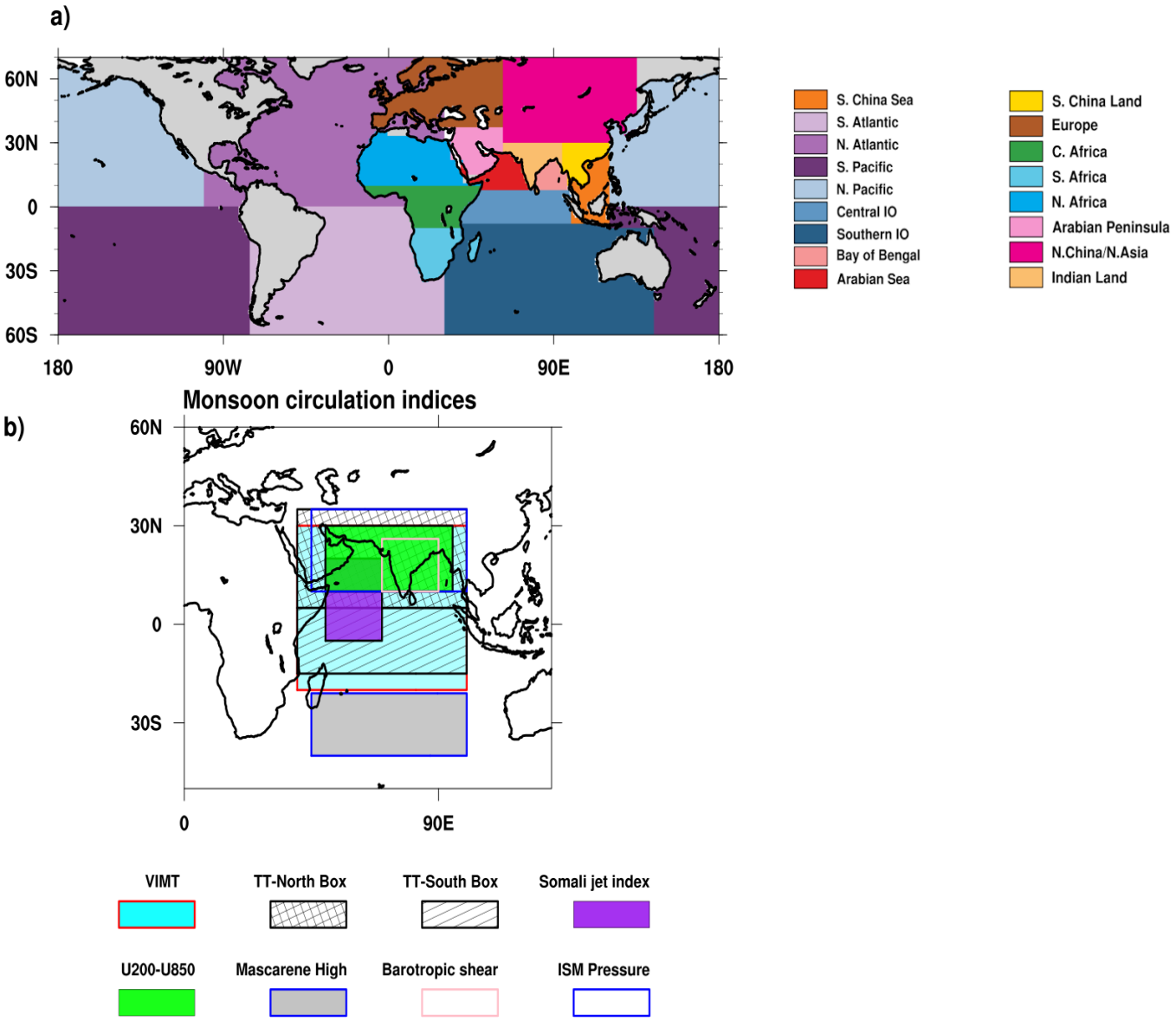

Figure S2: Panel a) shows the map of the 17 water vapor source regions for the Indian monsoon domain, used in the water tagging simulations. The tagged regions include major oceanic basins and key terrestrial areas. Gray regions on the map are not tagged.

Panel b) shows the geographical areas defining the monsoon circulation strength indices. 1) The hydrological index, calculated by averaging the Vertically Integrated Moisture Transport (VIMT) in the Indian Ocean-Arabian Sea region, [20°S-30°N, 40°E-100°E.

2) tropospheric temperature gradient (ΔTT) between the two boxes in the north (10°N-35°N, 30°-110°E) and south (15°S-10° N, 30°-110°E);

3) vertical shear of zonal winds (ms^{-1}) as the change between U at 200 hPa and U at 850 hPa averaged over the region (10°- 30°N, 50°E-95°E).

4) Somali jet speed index, calculated as the square root of twice the area-averaged kinetic energy of 850 hPa horizontal winds over the region (5°S-20°N, 50°E-70°E).

5) The mean sea-level pressure difference between the Mascarene high (MH; 20°S-40°S, 45°E-100°E) and the wider Indian summer monsoon region (10°N-35°N, 45°E-100°E, ISM pressure domain in panel b).

6) Barotropic shear (meridional shear of 850 hPa zonal wind ($\partial u/\partial y$) in S^{-1}) estimated over 10°N-26°N, 70°E-90°E.

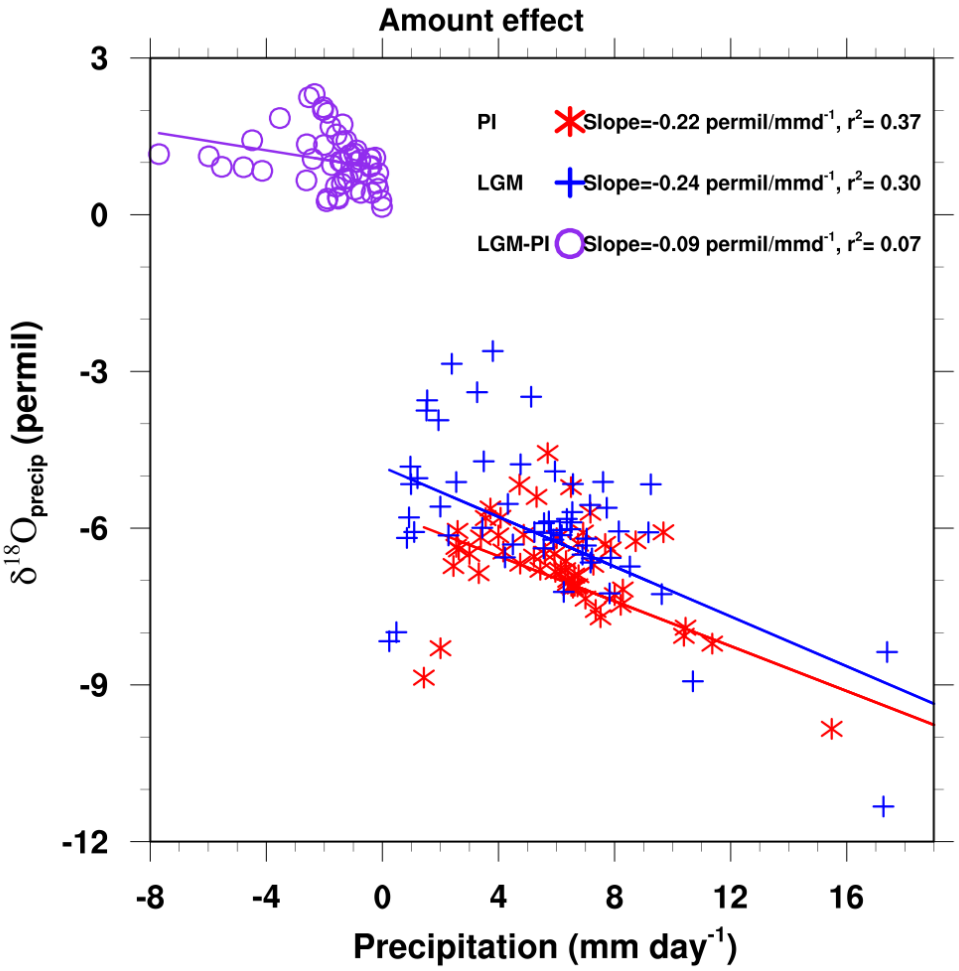

Figure S3. The amount effect over the Indian land region, shown as the linear regression between JJAS mean precipitation $\delta^{18}O_{precip}$ (in ‰) and precipitation rate (mm day^{-1}). The spatial relationship is shown for the PI simulation; red markers and line), the LGM simulation; blue markers and line. The linear regression between the differences of precipitation rate and $\delta^{18}O_{precip}$ between the two climate states, LGM-PI, the temporal relationship, is shown in purple colour markers and line. The slopes and regression coefficients r^2 (the square of the Pearson correlation coefficient r) from the regression analysis are shown in the panels.

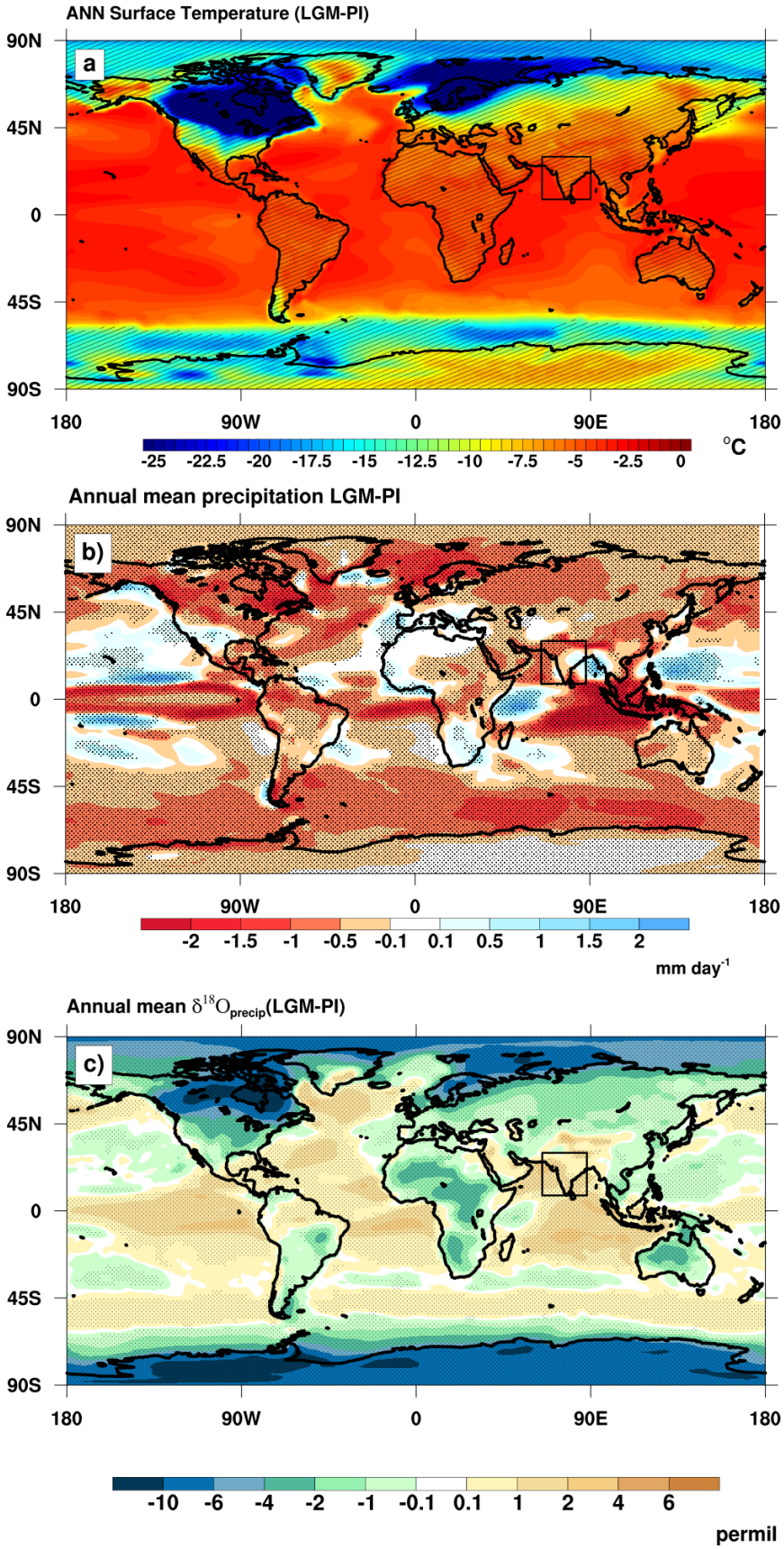

Figure S4. Simulated differences in the annual mean surface temperature, precipitation, and $\delta^{18}O_{precip}$ between the LGM and the PI runs. Panel (a) shows the

differences in surface temperature (in °C). Panel (b) shows the differences in precipitation (in mm day^{-1}), and panel (c) shows the differences in $\delta^{18}O_{precip}$ in permil. Regions where the anomalies are statistically significant at the 95% confidence level are hatched/stippled. Significance level is estimated using a Student's t test from a sample of 20 annual means from the control and LGM simulations.

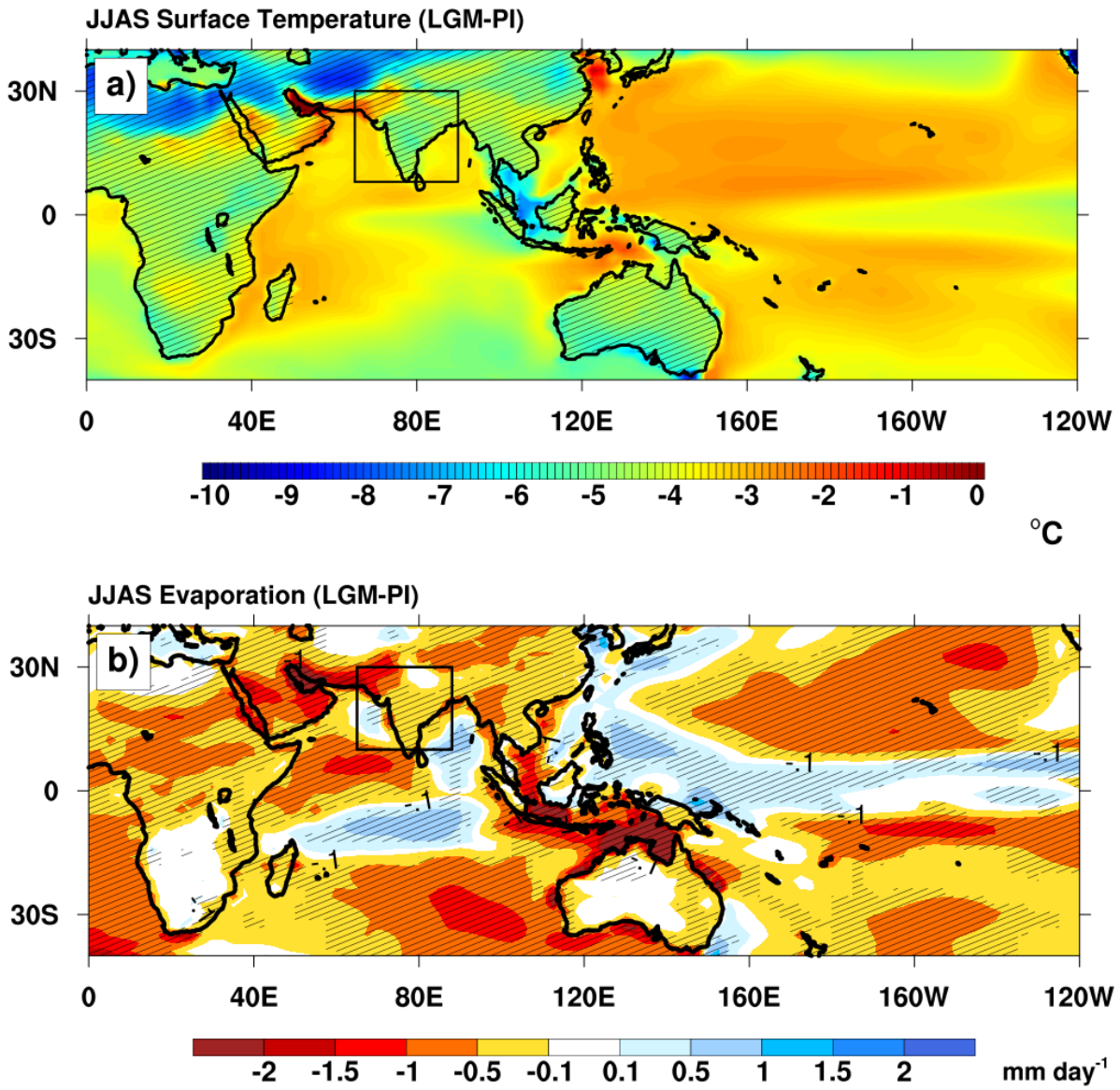

Figure S5. Simulated differences during the mean JJAS season between the LGM and the PI runs. Panel (a) shows the differences in surface temperature (°C). Panel (b) shows the differences in surface evaporation (mm day^{-1}). Regions where the anomalies are statistically significant at the 95% confidence level are hatched. Significance level is estimated using a Student's t test from a sample of 20 annual means from the control and LGM simulations.

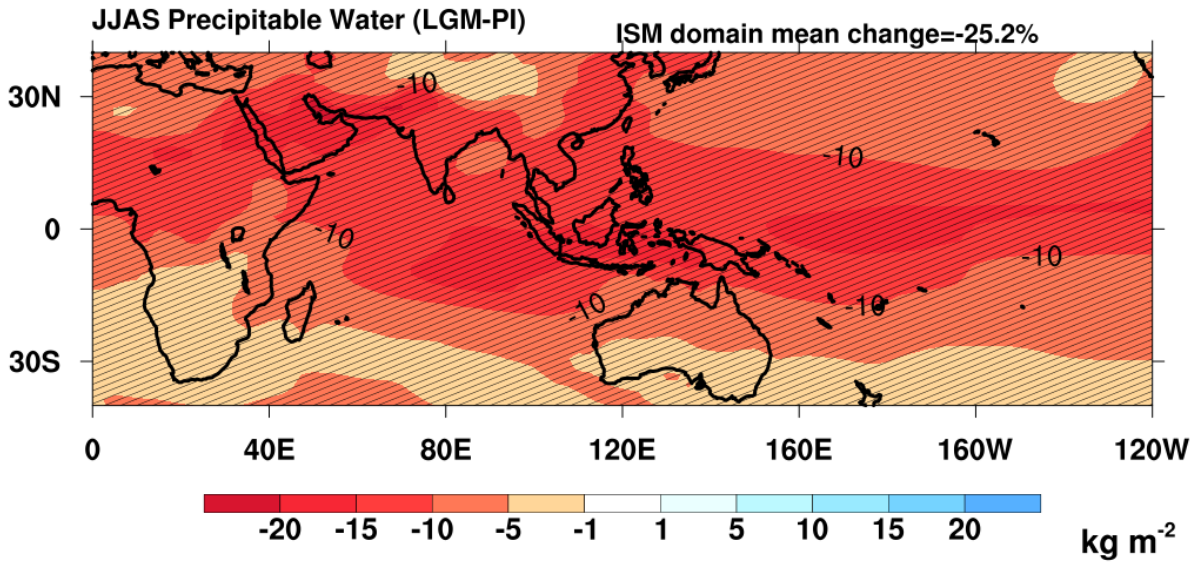

Figure S6. Difference in JJAS mean column precipitable water (in kg m^{-2}) between the LGM and PI simulations. Regions where the anomalies are statistically significant at the 95% confidence level are hatched. Significance level is estimated using a Student's t test from a sample of 20 annual means from the control and LGM simulations.

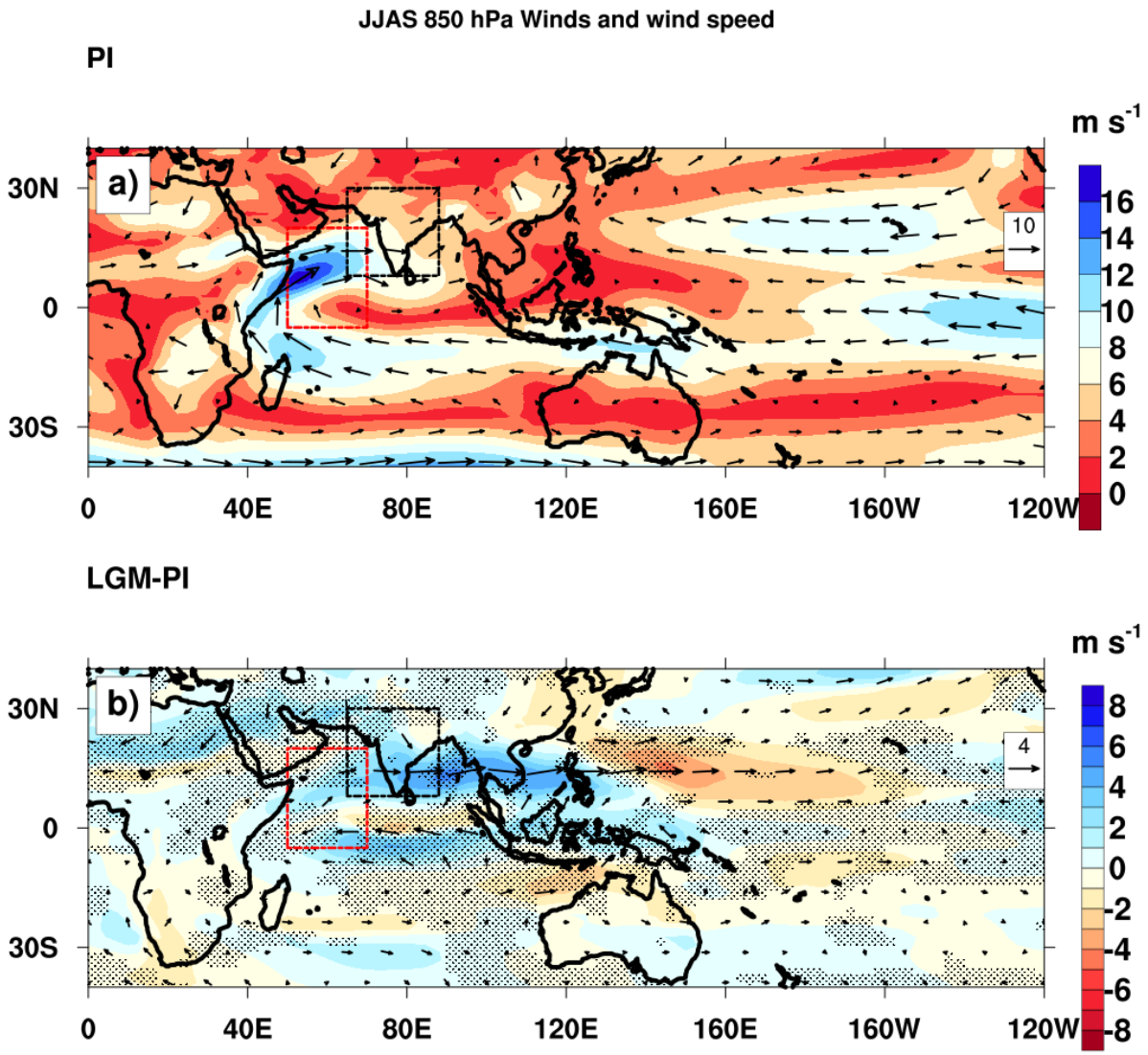

Figure S7. Simulated 850 hPa winds (m s^{-1}) and magnitude of wind speed for the JJAS season. In both panels, vectors represent wind direction, and the color shading indicates the magnitude of the wind speed. Panel (a) shows the absolute values for the PI simulation. Panel (b) shows the differences between the LGM and PI simulations (LGM-PI). Regions where the anomalies are statistically significant at the 95% confidence level are stippled. Significance level is estimated using a Student's t test from a sample of 20 annual means from the control and LGM simulations. The black box highlights the Indian monsoon domain (8°N-30°N, 65°E-88°E), and the red box shows the geographical region used to calculate the Somali Jet index (5°S-20°N, 50°E-70°E).

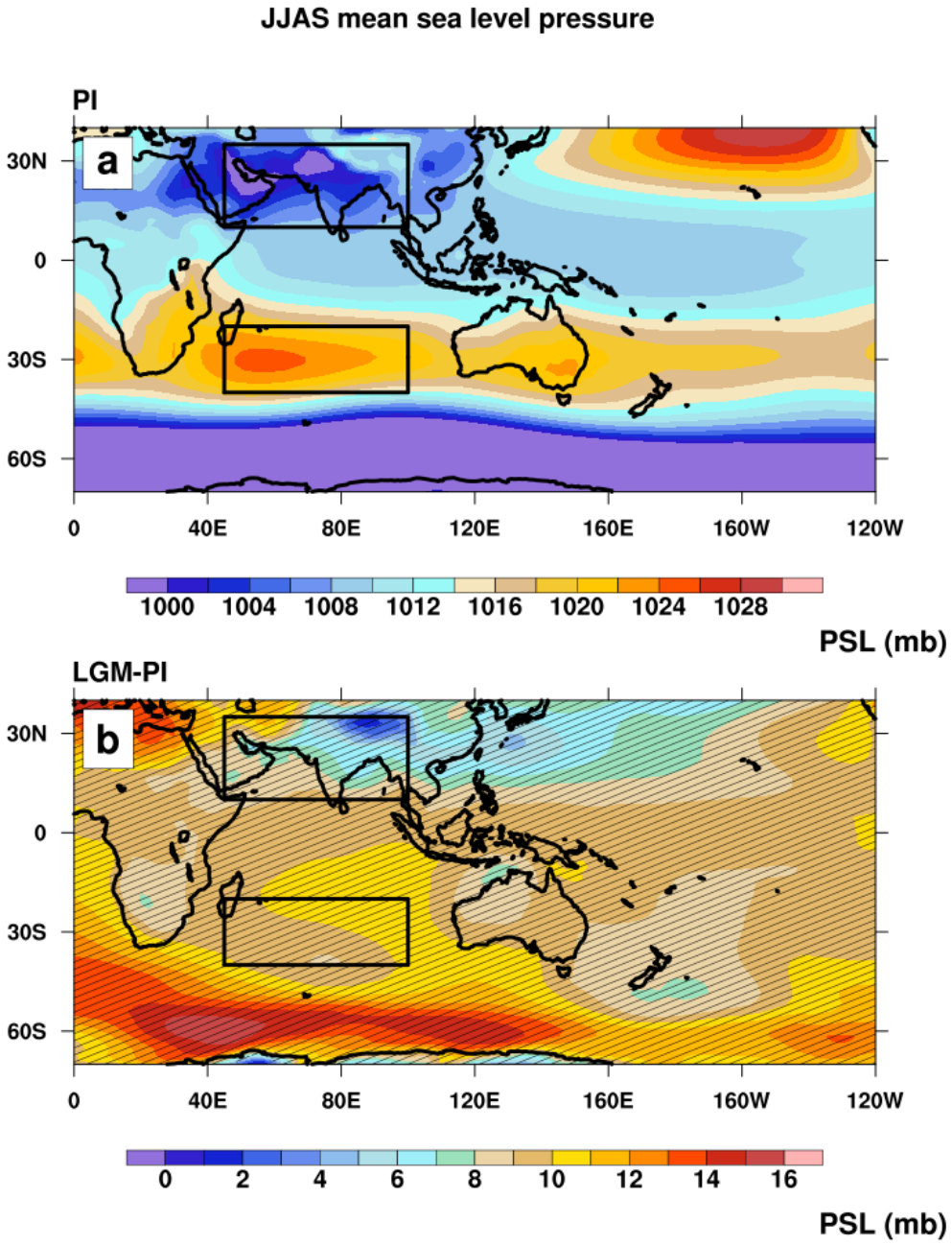

Figure S8. JJAS mean sea level pressure (PSL) in mb. Panel a) shows mean PSL for the Pre-Industrial simulation. Panel b) shows the difference in mean PSL between the LGM and PI simulations as (LGM-PI). The black boxes highlight the Mascarene high in the Southern Indian Ocean and Indian monsoon region in the north used to calculate the pressure gradient. Regions where the anomalies are statistically significant at the 95% confidence level are hatched. Significance level is estimated using a Student's t test from a sample of 20 annual means from the control and LGM simulations.

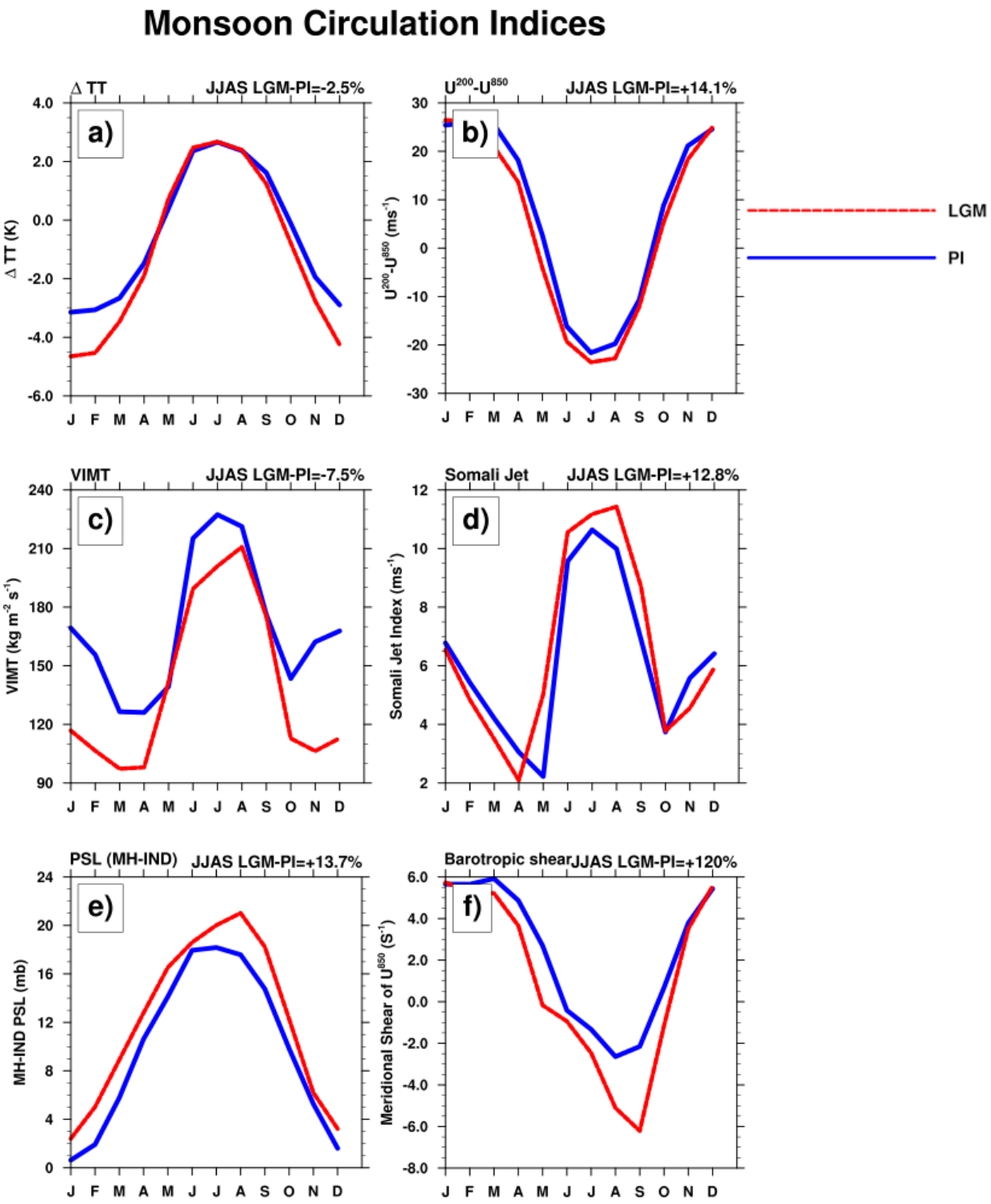

Fig. S9: Monsoon circulation Indices calculated from the monthly means of PI and LGM simulations. The geographical areas for the calculations are shown in Figure S2b. JJAS mean values of differences between LGM and PI as (LGM-PI) in % is shown in the right top of each panel.

Panel a) shows the tropospheric temperature gradient (ΔTT) between the northern box (10°N - 35°N, 30°-110°E) and the southern box (15°S - 10°N, 30°-110°E). **Panel b)** shows the vertical shear of zonal winds (u in m/s) calculated as the change between U850 and U200 (U850-U200) averaged over the region (10°N-30°N, 50°E-95°E). **Panel c)** shows the hydrological index, calculated by averaging the Vertically Integrated Moisture Transport (VIMT) in the Indian Ocean-Arabian Sea region, [20°S-30°N, 40°E-100°E. **Panel d)** shows Somali jet speed index, calculated as the square root of twice the area-averaged kinetic energy of 850 hPa horizontal winds over the region (5°S-20°N, 50°E-70°E). **Panel e)** shows the mean sea-level pressure difference between the Mascarene high (MH; 20°S-40°S, 45°E-100°E) and the wider Indian summer monsoon region (10°N-35°N, 45°E-100°E. **Panel f)** shows the barotropic shear estimated over 10°N-26°N, 70°E-90°E.

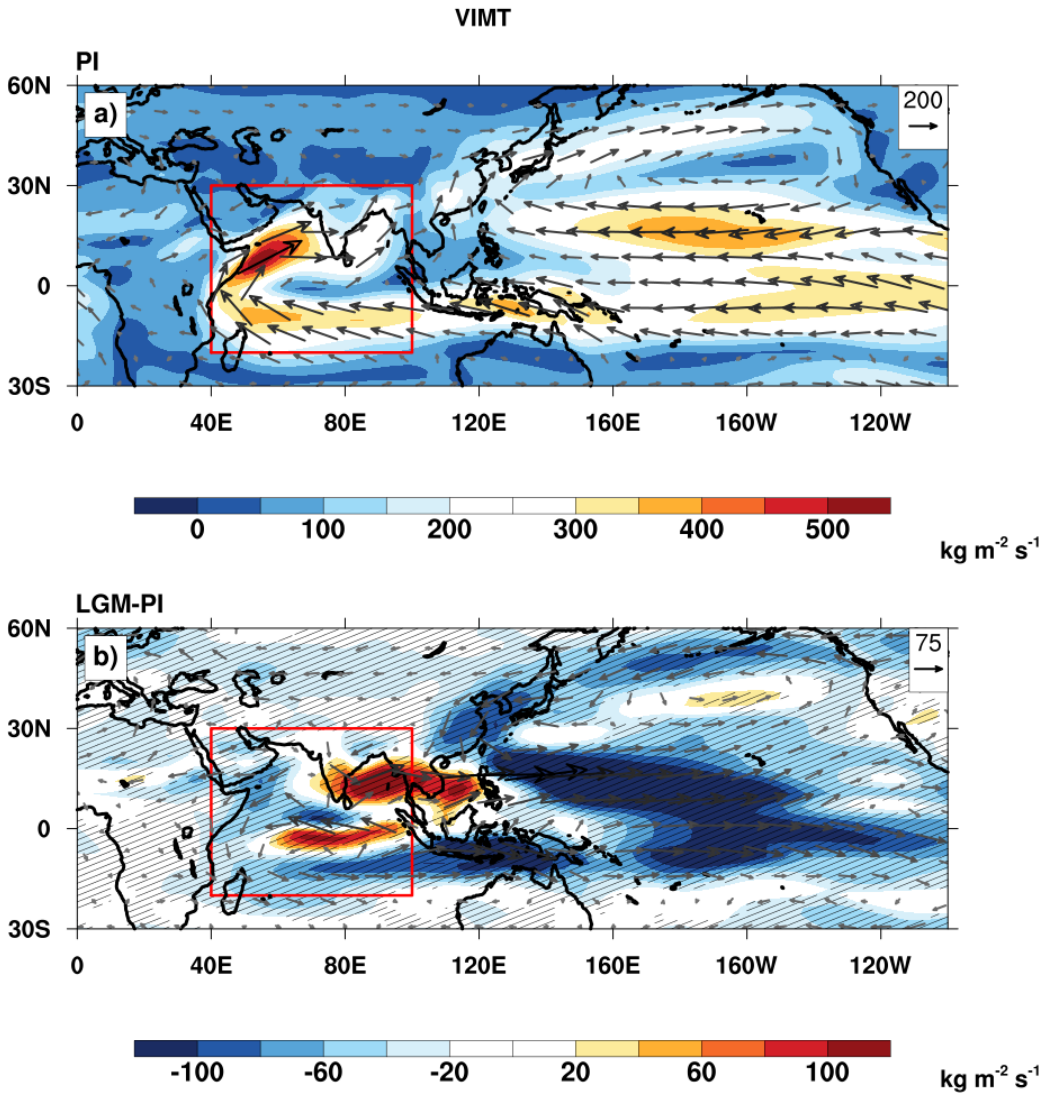

Figure S10. Vertically Integrated Moisture Transport (VIMT) from the surface to 300 hPa for the JJAS season. Panel (a) shows the VIMT for the PI simulation. Panel (b) shows the differences in VIMT between the LGM and the PI simulations (LGM-PI). In both panels, vectors indicate the direction and magnitude of moisture transport, while color shading represents the magnitude of the transport in kg m⁻2 s⁻¹. Regions where the anomalies are statistically significant at the 95% confidence level are hatched. Significance level is estimated using a Student's t test from a sample of 20 annual means from the control and LGM simulations. The red box denotes the geographical region used to calculate the monsoon hydrological index (mean of VIMT over the domain 20°S-30°N, 40°E-100°E).

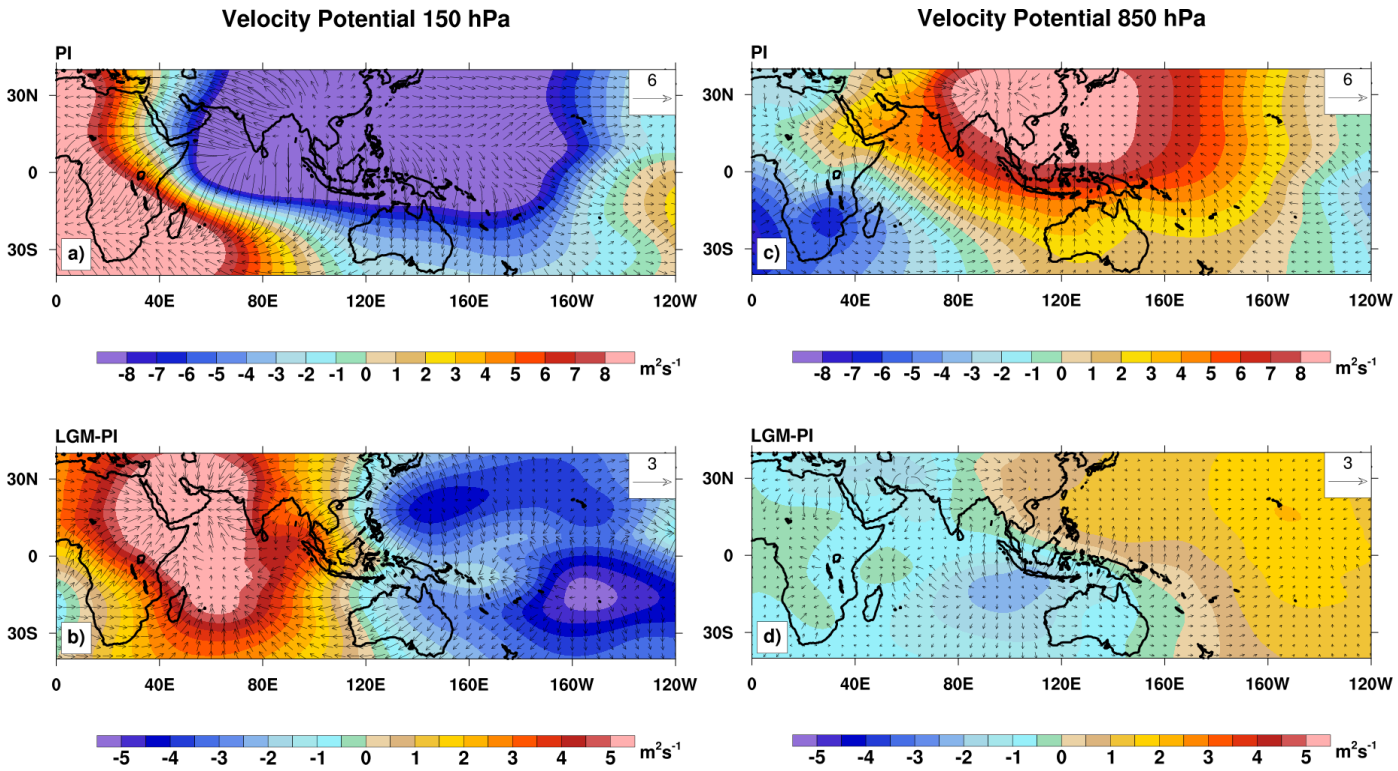

Figure S11: The JJAS mean 150 hPa (Panels a, b) and 850 hPa (Panels c, d) velocity potential (shaded, in m^2 s^{-1}) and divergent wind (vectors, ms^{-1}). The reference vectors are shown in the top right corner of each panel. Panels a) and c) show the absolute values of velocity potential and divergent wind for the PI simulation for the 150 hPa level and 850 hPa level, respectively. Panels b) and d) show the differences between the LGM and PI as LGM-PI for the 150 hPa level and 850 hPa level, respectively.

Panels a) and c) show the strong low-level convergence at 850 hPa (red shading) over the ISM region in regions of ascending motion (Monsoon regions and Western Pacific) in the PI, accompanied by strong upper-level divergence (blue shading) at 150 hPa. Panels b) and d) show anomalous low-level convergence (upper-level divergence) over the western Pacific and increased low-level divergence (upper-level convergence) over the Indian region in the LGM simulation.

Table S1: GHG and orbital boundary conditions for the simulations.

Experiment	GHG values	Orbital year
Pre-industrial control (PI)	CO_2 284.7 ppm, CH_4 791.6 ppb, N_2O 275.68 ppb	1850
LGM	CO_2 190 ppm, CH_4 375 ppb, N_2O 200 ppb	21 Ka BP

Table S2: Simulated anomalies (LGM minus PI) for June-July-August-September (JJAS) mean surface temperature (K) and surface evaporation (%) over the 17 tagged water vapor source regions.

Source region	Differences in variables over Source region (JJAS mean)	
	Surface temperature (LGM-PI) in K	Surface evaporation (LGM-PI) in %
Arabian Sea	-3.43	-11
Bay of Bengal	-3.88	-0.29
South Indian Ocean	-5.72	-13.94
Central Indian Ocean	-3.63	-6.27
North Pacific Ocean	-3.56	-6.8
South Pacific Ocean	-4.13	-9.36
North Atlantic Ocean	-5.09	-11.48
South Atlantic Ocean	-5.74	-17.78
South China Sea	-4.53	-13.85
Indian land (Recycling)	-4.35	-17.11
N.China and N.Asia	-5.57	-26.15
Arabian Peninsula	-5.04	-47.38
Northern Africa	-5.49	-22.26
Southern Africa	-4.33	-6.97
Central Africa	-4.71	-14.89
Europe	-9.10	-34.84
South China land region	-4.40	-9.72